Vol. 7 • No. 12 • June 23 • 2020

www.advmatinterfaces.de

ADVANCED MATERIALS INTERFACES

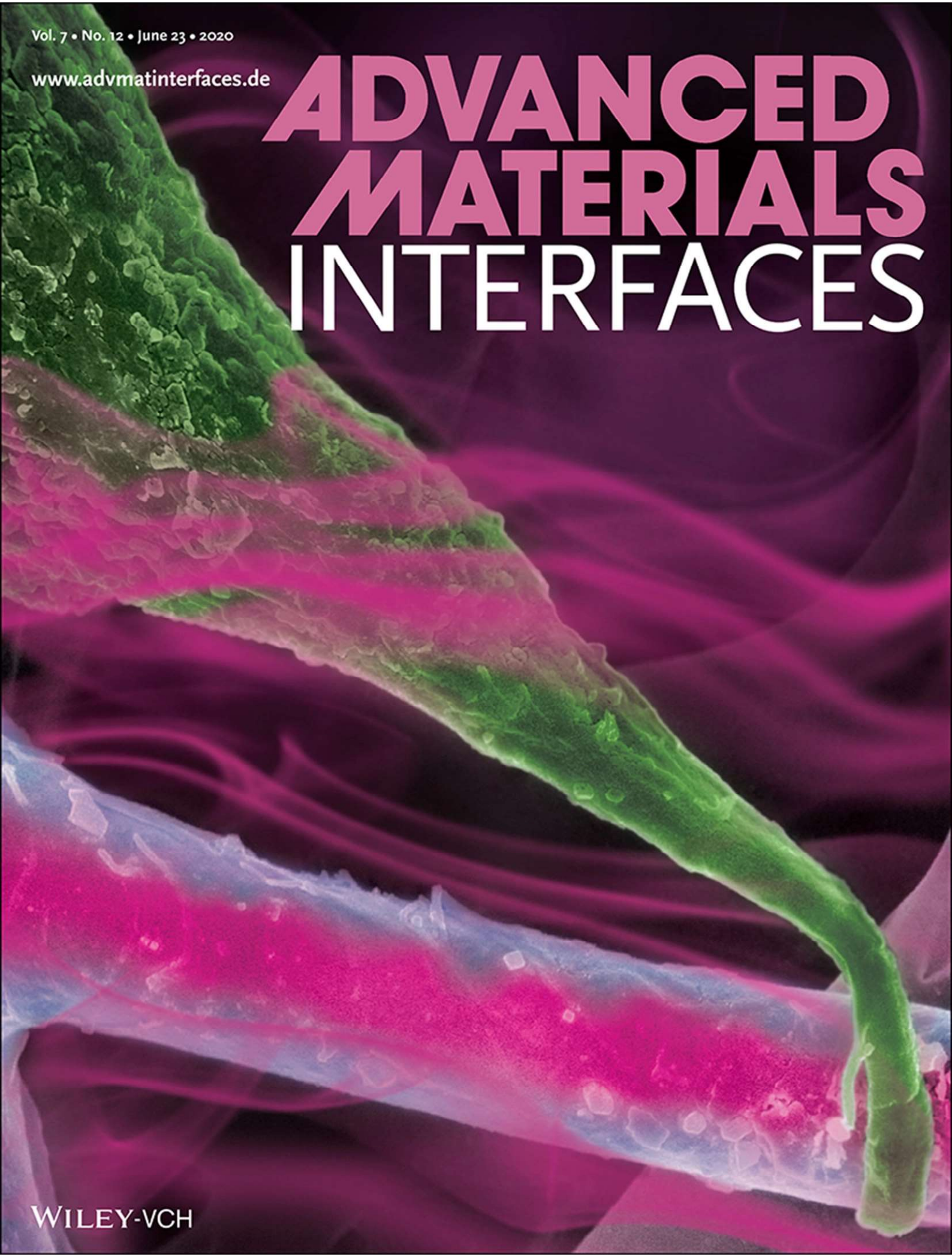

WILEY-VCH

ADVANCED MATERIALS INTERFACES
www.advmatinterfaces.de

Ultraviolet Light-Assisted Electrospinning of Core–Shell Fully Cross-Linked P(NIPAAm-*co*-NIPMAAm) Hydrogel-Based Nanofibers for Thermally Induced Drug Delivery Self-Regulation

*Sylwia Pawłowska, Chiara Rinoldi, Paweł Nakielski, Yasamin Ziai, Olga Urbanek, Xiaoran Li, Tomasz Aleksander Kowalewski, Bin Ding, and Filippo Pierini**

Body tissues and organs have complex functions which undergo intrinsic changes during medical treatments. For the development of ideal drug delivery systems, understanding the biological tissue activities is necessary to be able to design materials capable of changing their properties over time, on the basis of the patient's tissue needs. In this study, a nanofibrous thermal-responsive drug delivery system is developed. The thermo-responsivity of the system makes it possible to self-regulate the release of bioactive molecules, while reducing the drug delivery at early stages, thus avoiding high concentrations of drugs which may be toxic for healthy cells. A co-axial electrospinning technique is used to fabricate core–shell cross-linked copolymer poly(*N*-isopropylacrylamide-*co*-*N*-isopropylmethacrylamide) (P(NIPAAm-*co*-NIPMAAm)) hydrogel-based nanofibers. The obtained nanofibers are made of a core of thermo-responsive hydrogel containing a drug model, while the outer shell is made of poly-L-lactide-*co*-caprolactone (PLCL). The custom-made electrospinning apparatus enables the in situ cross-linking of P(NIPAAm-*co*-NIPMAAm) hydrogel into a nanoscale confined space, which improves the electrospun nanofiber drug dosing process, by reducing its provision and allowing a self-regulated release control. The mechanism of the temperature-induced release control is studied in depth, and it is shown that the system is a promising candidate as a "smart" drug delivery platform.

1. Introduction

The biological activities of the human body are various, complex, and dependent on several factors, so biological processes change dynamically over time. Biomaterials have quite often been designed to deal with specific problems without taking into account the mutability of biological tissue activities and needs over time.[1] This issue has seriously affected the development of drug delivery systems which are frequently based on the belief that "extended" and "sustained" are synonymous with an "optimal" release.[2] Several nanostructured biomaterials have been developed to meet those requirements, obtaining materials able to release drugs over the long term, without taking into account the optimization of the bioactive molecule secretion level at the first stage after implantation.[3] This problem is intrinsic to polymer nanomaterials since, due to the very high surface area to volume ratio, they release a considerable quantity of drug, which can easily exceed the therapeutic range.[4] It is worth remembering that the amount of drugs in body fluids should be kept at the therapeutic level, which is a concentration expected to be efficient without causing problems to the patient.[5] Therefore, there is an urgent need for the development of systems capable of delivering desirable amounts of drugs in a controlled manner, thus making it possible to maintain a concentration of bioactive molecules that matches the therapeutic range.[6] Consequently, a good deal of effort has been put into drug delivery research, seeking to improve the therapeutic effectiveness and reduce the side effects of drugs, while targeting clinical requirements.[7]

The development of smart biomaterials is another step toward the production of fully biomimetic materials, by tailoring and tuning material properties on the basis of the needs of the biological tissue at a specific time.[8–10] Stimuli-responsive drug delivery systems are materials characterized by large reversible, physical, and/or chemical changes in response to

Dr. S. Pawłowska, C. Rinoldi, Dr. P. Nakielski, Y. Ziai, Dr. O. Urbanek, Prof. T. A. Kowalewski, Dr. F. Pierini
Department of Biosystems and Soft Matter and Laboratory of Polymers and Biomaterials
Institute of Fundamental Technological Research, Polish Academy of Sciences
Warsaw 02-106, Poland
E-mail: fpierini@ippt.pan.pl
Prof. X. Li, Prof. B. Ding
State Key Laboratory for Modification of Chemical Fibers and Polymer Materials
Innovation Center for Textile Science and Technology
Donghua University
Shanghai 200051, China
The ORCID identification number(s) for the author(s) of this article can be found under https://doi.org/10.1002/admi.202000247.

DOI: 10.1002/admi.202000247

condition variations.[11] The responsiveness opens the door for the development of novel materials with controllable physical properties such as stiffness, wettability, and release of specific molecules.[12–15] Stimuli-responsive drug delivery systems featuring sustained and controlled drug release are highly desirable because they can deliver the requested active molecule dose while avoiding unwanted cell uptake.[16] This concept underscores the fact that for the adjustment of drug release, more sophisticated systems than simple nanomaterial-embedding drugs are necessary, because changes and related timing are crucial factors in most biological processes.

Hydrogels are defined as a group of polymeric materials which have a water-insoluble hydrophilic structure; this structure enables them to retain large amounts of water in their 3D networks, thus endowing them with physical properties similar to those of soft living tissues.[17] Hydrogels have outstanding tunable mechanical properties and are biocompatible; moreover, they are non-irritant thanks to their hydrophilic nature.[18,19] Additionally, it is worth pointing out that the high quantity of water in the system makes it possible to use them as efficient carriers in drug delivery systems.[20,21] Polymer hydrogels are still a new, rapidly developing group of materials, which are considered promising candidates for a number of applications in many different fields.[22–24] They are used extensively to design advanced biomaterials with controlled physical, chemical, and biological properties that make them particularly suitable for mimicking and stimulating biological tissues.[25,26] One of the most interesting hydrogel classes for biomedical applications is that of polyacrylate hydrogels, particularly poly(*N*-isopropylacrylamide) (PNIPAAm), because of their ability to swell and contain an enormous amount of water within their network. PNIPAAm-based hydrogels are proven to be stable in physiological body conditions; moreover, they are non-toxic, non-inflammatory, and their viscoelasticity is comparable with that of the surrounding soft living tissues.[27–29] Additionally, PNIPAAm is particularly attractive due to its responsivity depending on temperature.[30,31]

System miniaturization and structuration at the nanoscale level play essential roles in developing materials for biomedical applications.[32–35] Material scientists are focusing their attention on materials that can mimic the architecture of the extracellular matrix (ECM), which can facilitate the development of artificial functional tissues, improving cell–material interaction.[36–39] Among several methods for producing fibrous polymer materials, electrospinning has gained great interest thanks to its potential and innovations and, at present, it is the only technique capable of producing real nanometric fibrous structures with high porosity.[40–45]

Up to now, the scientific community has developed and investigated the function of PNIPAAm-based nanofibers using uncross-linked PNIPAAm or blending polyacrylate derivatives with an electrospinnable polymer, as well as by embedding nanofibers in PNIPAAm bulk hydrogels.[46–49] Still, at the present time, fully cross-linked electrospun PNIPAAm-based hydrogel nanofibers have not yet been successfully fabricated.

In this work, we report the development of the first method capable of producing fully cross-linked PNIPAAm-based hydrogel nanofibers using electrospinning. This innovative process is based on the use of a co-axial electrospinning setup to obtain a cross-linked hydrogel core confined within an electrospinnable polymer shell. Our research effort was first devoted to overcoming the difficulties faced during the design of core–shell fibers by co-axial electrospinning, while paying special attention to the challenges related to the electrospinning of water-like monomer solutions. In this frame, the system we propose appears particularly original due to its novel core–shell structure. Indeed, it has been designed to possess a thermoresponsive hydrogel core, while generally core–shell fibers have been more easily developed having hydrogel shell.[50,51] Moreover, PNIPAAm-based core–shell structures, which are typically considered for tissue engineering purposes, here are introduced as drug delivery platforms, exploiting the advantage of having a polymeric shell barrier. Thus, the higher level of fabrication difficulties is rewarded by achieving an optimized release rate when compared to simple fibrous constructs.[52] The morphology, structure, and chemical properties of the electrospun core–shell fibers were characterized in depth by comparing them with poly-L-lactide-*co*-caprolactone (PLCL) nanofibers. In vitro experiments clearly prove the benefit provided by the developed nanostructures in terms of material interactions with living cells. Moreover, in vitro drug release tests show that the initial release of drug model molecules from hydrogel-based core–shell fibers is remarkably slower than in pure PLCL systems, while the drug delivery is optimized even at the late release stage.

2. Results and Discussion

2.1. Core–Shell Nanofibers Fabrication by Light-Assisted Co-Axial Electrospinning

PNIPAAm-like hydrogels are a very popular class of smart thermo-responsive materials. Due to their chemical and structural features these polymers respond to temperature variations in a range close to that of the human body. Because of the high biocompatibility these hydrogels become one of the most attractive biopolymer families.[53]

Electrospinning can be applied to a wide range of polymers, provided that the polymer solution exceeds a critical value of molecular weight, viscosity, and concentration sufficient to obtain nanofibers.[42] Unfortunately, it is very difficult to electrospin *N*-isopropylacrylamide-*co*-*N*-isopropylmethacrylamide (NIPAAm-*co*-NIPMAAm) hydrogel precursor solutions because these systems (mainly made of small molecules in water) do not meet the chemical and physical requirements necessary to be considered electrospinnable. The fabrication of hydrogel fibers is now possible thanks to the implementation of an innovative electrospinning-based method able to confine a hydrogel core into a polymer shell. The enclosure of hydrogel in the form of nanofibers is possible due to the use of a PLCL shell (70% L-lactide and 30% caprolactone). The fabricated core–shell nanostructures consist of a PLCL shell and a fully cross-linked poly(*N*-isopropylacrylamide-*co*-*N*-isopropylmethacrylamide) (P(NIPAAm-*co*-NIPMAAm)) hydrogel for self-regulated drug delivery with rapid responsiveness to temperature. **Figure 1** schematically shows core–shell fiber fabrication via electrospinning. The custom-developed electrospinning setup as well as core–shell needle system play a vital role in solving this

specific issue, allowing a formation of a core–shell Taylor cone (Figure S1a, Supporting Information).

It is vital to keep the temperature below the hydrogel lower critical solution temperature (LCST) during the electrospinning in order to obtain a defect-free and homogeneous hydrogel structure.[54,55] This is because uncross-linked PNIPAAm-based systems are miscible with water at low temperature, but a typical phase separation followed by precipitation occurs when the characteristic LCST is exceeded.[56] However, the cross-linking of PNIPAAm chains makes it possible to obtain hydrogels that convert precipitation behavior into a significant structural modification of the polymer chain network, resulting in shrinking, stiffening, and reduction in volume and porosity (Movie S1, Supporting Information). This structural changes of PNIPAAm takes place at approximately 33 °C. However, it can be increased by copolymerizing NIPAAm with its derivative NIPMAAm, which has additional hydrophobic groups in the polymer chains.[57–60] Adding a second monomer, in order to set the LCST at around 37 °C, allows achieving an effective drug release responsivity in physiological condition (Figure S1b, Supporting Information).

The fabrication of polymeric fibers through electrospinning requires great attention to numerous parameters that affect the final structure of the fiber.[42] In the case of core–shell fibers, where the core is a non-polymerized hydrogel precursor solution in the initial stage of fiber formation, the number of such parameters increases. The attention to these parameters is crucial to obtain a material with the desired structure. In this work, concentration of PLCL and hydrogel precursor solutions have been previously optimized in order to obtain a regular and defect-free fiber structure. The hydrogel precursor is loaded with a small amount of Rhodamine B (RhB) as a drug model for the drug delivery test and oxygen molecules are removed by bubbling with Argon gas upon starting the polymerization reaction (Figure 1a). Solutions are then loaded into syringes and mounted into a closed double-walled chamber, which makes it possible to perform the electrospinning process in strictly defined environmental conditions (Figure 1b). Thanks to the addition of a cooling system to the chamber, it is possible to control temperature and humidity. The cooling unit, which consists of a refrigerator, a heat exchanger, and a fan embedded in the electrospinning apparatus, makes it possible to reach a stable temperature up to −10 °C in the spinning area (Figure S1c, Supporting Information). The possibility of controlling environmental parameters during the electrospinning of our polymer system is fundamental because if

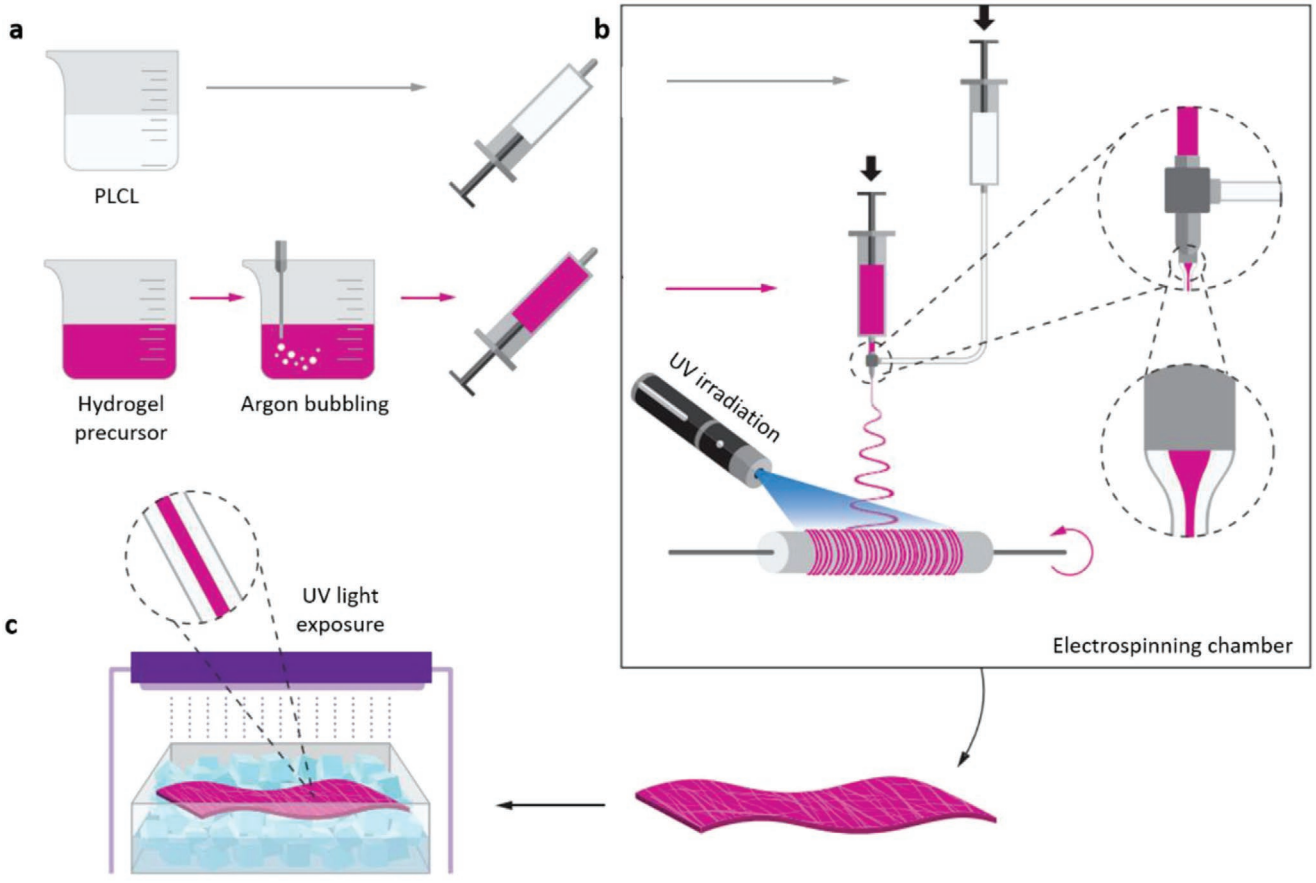

Figure 1. Schematic of core–shell fiber production. a) NIPAAm-*co*-NIPMAAm hydrogel precursor loaded with RhB is degassed by Argon bubbling and loaded into a syringe and connected to a core–shell needle as the core solution. PLCL solution is loaded into a syringe and connected to the core–shell needle as the shell solution. b) Formation of electrospun core–shell fibers into the electrospinning chamber. The solutions flow from the needle tip and the resulting fibers are collected onto a rotating drum while irradiated with UV light. c) The obtained electrospun matrix is placed in ice, and exposed to UV light to allow the cross-linking of the hydrogel component and obtain P(NIPAAm-*co*-NIPMAAm)-PLCL core–shell fibers.

the polymerization takes place at temperatures higher than the LCST, the hydrogel structure shrinks, transitioning to a globular structure which, in turn, generates structural inhomogeneity. In this situation the material is not transparent but opaque, expels most of its water, and loses most of the physical change potential that will take place during the LCST transition (Figure S1d, Supporting Information). On the other hand, too low temperature in the chamber may interfere with the solvent evaporation process during the formation of the PLCL shell. Therefore, the use of a temperature controller offers the possibility of achieving a balance between these two important aspects for the electrospinning of this challenging core–shell system. Humidity control is also a standard procedure in the electrospinning process. It is well-known that during the electrospinning of polymeric solutions with an organic solvent humidity should not exceed 50–60%, in order to prevent the formation of fiber defects.[61] However, in case of water-like solutions it is necessary to increase the humidity to around 70% in order to avoid the unwanted water loss associated with the evaporation from the fiber structure and compensating for this loss of water. In the spinning of a core aqueous solution, water is trapped in the hydrogel network as a result of polymerization. A key factor in the nanostructure fabrication is the in situ hydrogel polymerization, which should be carried out before the core solution leaks and/or evaporates from the nanofiber structure. Therefore, while fibers are collected on a rotating drum, a free-radical polymerization of P(NIPAAm-*co*-NIPMAAm) hydrogel was activated by simultaneous use of both chemical and ultraviolet (UV) light irradiation pathways (Figure 1b). In this perspective, another improvement in the operation of the electrospinning chamber and electrospinning process was the irradiation of just-spun fibers by UV light, which is necessary to trigger the polymerization reaction of the hydrogel core structure. Immediate polymerization prevents the escape of the aqueous solution (which has low viscosity) from the fiber centers through any possible cracks in the shell structure. Similar in situ UV irradiation tactics were used by Lin and Tsai in their studies on UV-cross-linking gelatin electrospun fibers.[62] It is worth pointing out that a small amount of ammonium persulfate (APS) combined with thetramethylenediamine (TEMED) was added to the core solution to slowly catalyze the polymerization. This process improves the quality and the stability of the final structure by increasing the core solution viscosity during the electrospinning process. In addition, in order to ensure the complete polymerization, a post-electrospinning UV irradiation was performed in ice, retaining the temperature below LCST (Figure 1c).

2.2. Morphological and Structural Properties of Hierarchically Architectured Nanofibers

The schematic of core–shell fibers composed of P(NIPAAm-*co*-NIPMAAm) hydrogel core and PLCL shell is reported in **Figure 2**a. The morphology of the fibers was characterized using various imaging techniques in order to investigate the fiber composition and structure. Fluorescence imaging was used first of all to assess the presence of a fluorescent core and the regularity of the core–shell structure. Fluorescence micrographs combined with bright-field images showed a continuous fluorescent hydrogel fibrous core surrounded by a transparent PLCL shell (Figure 2b). These results were confirmed by the images obtained using transmission electron microscopy (TEM). Indeed, TEM investigations clearly showed the presence of internal structures within the fibers (core), as can be seen in Figure 2c.

The morphological analysis performed by scanning electron microscopy (SEM) of core–shell and pure PLCL fibers showed significant differences in fiber shapes (Figure 2d). In the case of pure PLCL fibers, a standard cylindrical shape of the fibers was observed, while core–shell fibers were more flattened, displaying ribbon-like shapes.[63] This is due to the collapse of the central part of the fiber core that occurs when the water from the hydrogel evaporates during the preparation of SEM analysis sample. Figure 2e shows SEM images of a partially dissolved shell of the core–shell fibers obtained by treating the fibrous material with *N*,*N*-dimethylformamide (DMF). Figure 2e shows the core–shell fiber at the solvent drop border, with a trace of core in the area where the shell of core–shell fibers was dissolved. The selective shell removal makes it possible to directly visualize the core structure.

To determine the dimension of the hydrated core–shell fibers, atomic force microscope (AFM) analysis was carried out (Figure 2f). Due to long-term sample incubation in deionized water before the AFM imaging, it was possible to measure the diameter of core–shell fibers with a completely hydrated hydrogel core. The values of core–shell and PLCL fiber diameters obtained on the basis of AFM measurements were as follows: 1.40 ± 0.13 and 1.40 ± 0.3 μm, respectively. Thus, it can be seen that the hydrated core–shell fibers are comparable in size to PLCL fibers. This is a significant advantage, because the dimension of core–shell fibers did not exceed that of PLCL fibers. Indeed, the fiber dimension might affect the release rate: the larger the diameter of fibers, the longer the diffusion path of drug molecules embedded into the fiber polymer matrix, thus resulting in a longer time for diffusion onto the surface of the fibers. On the other hand, smaller fibers have a higher surface area to volume ratio, which accelerates the molecule release from nanomaterials. Finally, core–shell and PLCL fibers were designed to have similar dimensions and, in turn, to allow a quantitative comparison of fibers in terms of the rate of dye molecule release from their structure, which is described in detail in Section 2.4.

Differential scanning calorimetry (DSC) and wide angle X-ray scattering (WAXS) were used to investigate the structure of the analyzed materials, while Fourier transform infrared (FTIR) spectroscopy was performed to confirm the presence of the hydrogel component into the core–shell fibers. DSC thermogram of the investigated P(NIPAAm-*co*-NIPMAAm) hydrogel shows a broad endothermic peak having the maximum at around 37 °C (**Figure 3**a). The LCST of NIPAAm and NIPMAAm are 32 and 42 °C, respectively. NIPMAAm molecules have different steric hindrance and hydrophilicity than NIPAAm, therefore NIPMAAm amount in the co-polymer chemical structure allows shifting the phase transition temperature toward higher values.[58] Polymerizing NIPAAm with another monomer containing a slightly different lateral group is one of the most common way to modify the phase transition

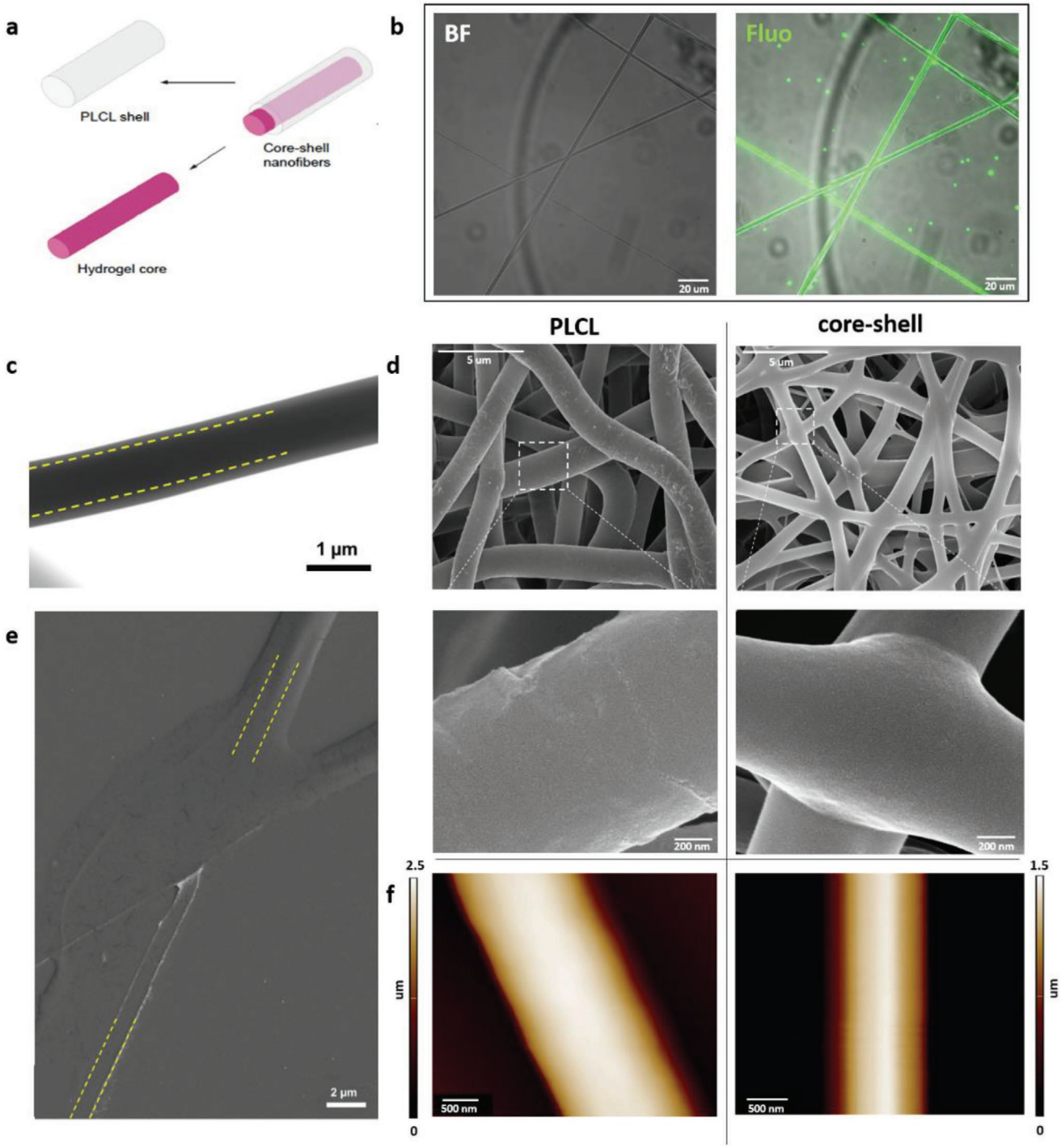

Figure 2. Morphology of P(NIPAAm-*co*-NIPMAAm)-PLCL core–shell fibers. a) Schematic of core–shell fibers composed of P(NIPAAm-*co*-NIPMAAm) core and PLCL shell. b) Images of fluorescent P(NIPAAm-*co*-NIPMAAm)-PLCL core–shell fibers: regular core–shell structure with a fluorescent green hydrogel core and transparent shell. c) TEM image of P(NIPAAm-*co*-NIPMAAm)-PLCL core–shell fiber: the presence of an internal core structure is visible within the fiber. d) SEM images of PLCL and P(NIPAAm-*co*-NIPMAAm)-PLCL core–shell fibers: the two materials reported different fiber shapes, cylindrical shape for PLCL fibers, flatter and ribbon-like shape for P(NIPAAm-*co*-NIPMAAm)-PLCL core–shell fibers. e) SEM image of a partially dissolved shell of core–shell fibers with visible the internal core structure. f) AFM topographic images of PLCL and P(NIPAAm-*co*-NIPMAAm)-PLCL core–shell fibers.

temperature. The presence of methyl groups in the main chain worsens the hydrophobic interaction, which means that a higher temperature value is needed to trigger the structural changes. The NIPAAm:NIPMAAm monomer ratio is proportional to the shift value and the higher is the NIPMAAm content in the copolymer, closer to 42 °C the phase transition temperature is.[56] In our case, the molar percentage of NIPMAAm was equal 3%, so the LCST should increase to 33–34 °C if compared

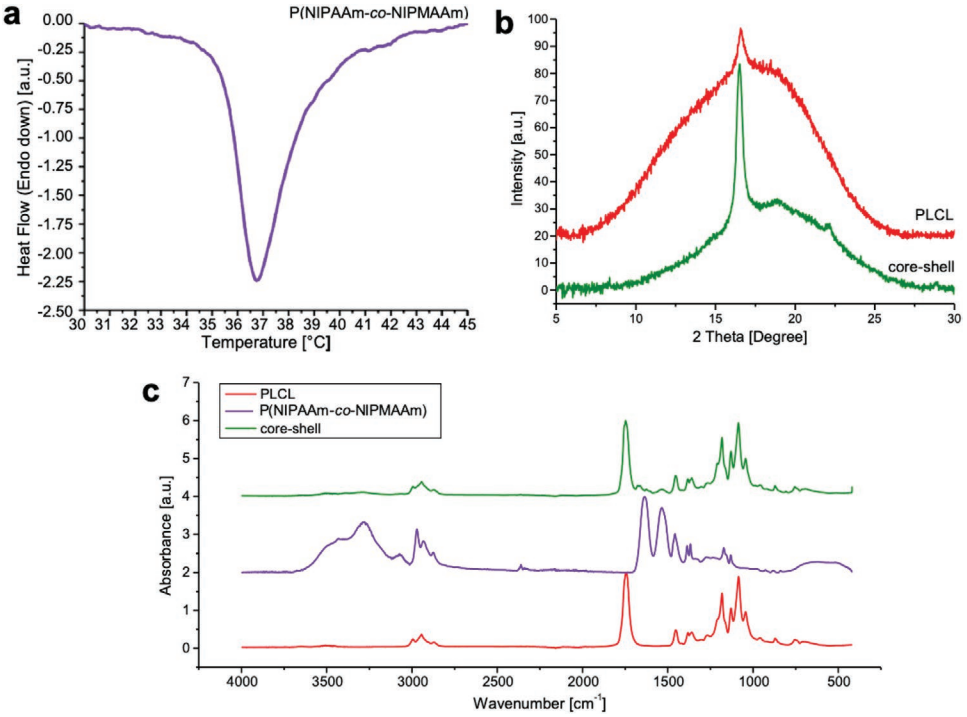

Figure 3. Chemical and structural properties of P(NIPAAm-*co*-NIPMAAm)-PLCL core–shell fibers. a) DSC of P(NIPAAm-*co*-NIPMAAm) shows the shift of the LCST from the typical 33 °C of PNIPAAm hydrogel to around 37 °C due to the addition of NIPMAAm in the precursor solution. b) WAXS spectra of P(NIPAAm-*co*-NIPMAAm)-PLCL core–shell fibers having additional, slightly shifted and masked peaks compared to the spectra of PLCL fibers, due to the amorphous structure of P(NIPAAm-*co*-NIPMAAm). c) FTIR graph of P(NIPAAm-*co*-NIPMAAm)-PLCL core–shell fibers having the characteristic peaks of PNIPAAm hydrogel, proving its presence in the final core–shell structure.

to uncross-linked PNIPAAm-based polymer chains.[56,57] The higher value of LCST obtained in our case is associated with an additional effect due to the presence of cross-linker molecules (BIS-AAm) in the hydrogel structure.[58,59] Therefore, the chemical and structural modifications associated with the presence of BIS-AAm allows to customize the LCST value of PNIPAAm-based systems, causing an additional shift of the phase transition temperature. This strategy allows to adjust the copolymer phase transition setting it at a temperature close to that of the human body.[56,58]

Wide-angle X-ray scattering (WAXS) spectra of PLCL nanofibers showed three characteristic intense peaks at 2θ = 14.1°, 16.6°, and 19.2°, indicating the presence of crystalline domains in the copolymer (Figure 3b).[64] The WAXS spectrum of the core–shell P(NIPAAm-*co*-NIPMAAm)-PLCL structure showed additional peaks which were slightly shifted and masked by the halo of the amorphous hydrogel structure (Figure 3b).[65,66] The degree of crystallinity for PLCL and core–shell materials was quantified by analyzing the WAXS diffractograms, obtaining crystallinity values of 1.5% and 11%, respectively. The higher degree of crystallinity in the core–shell structure is due to the influence of water content and high humidity in the system, which slows down the solvent evaporation and, in turn, promotes the formation of crystalline domains.

The FTIR spectra of PLCL and P(NIPAAm-*co*-NIPMAAm)-PLCL (core–shell) fibers are shown in Figure 3c. Moreover, the spectra of pure P(NIPAAm-*co*-NIPMAAm) hydrogel are shown for comparison of their characteristic peaks with those present in the core–shell structure. FTIR results showed the characteristic P(NIPAAm-*co*-NIPMAAm) absorption peaks at: 3390, 3295, and 3073 cm^{-1}, which are assigned to the N—H stretching of the secondary amine. Peaks at 1677 and 1538 cm^{-1} are also registered and can be attributed to the C=O stretching mode of amine (N—C=O).[67–70] The FTIR spectra of PLCL show three absorption peaks at 2996, 2946, and 2868 cm^{-1} corresponding to alkyl group vibrations, as well as a peak at 1744 cm^{-1} attributed to a COOR groups, and two peaks at 1183 and 1085 cm^{-1} attributed to C—O stretching vibration in PLCL.[64,71] The FTIR spectroscopy results confirm that P(NIPAAm-*co*-NIPMAAm) was incorporated into the final material core–shell structure. In the graph of core shell fibers (Figure 3c), the peaks from both P(NIPAAm-*co*-NIPMAAm) and PLCL can be observed, confirming the presence of both polymers in the core–shell structure (Table S1, Supporting Information).

2.3. Biomimetic Nanostructuration Supporting Polymer–Cell Interaction, Cell Viability, and Integration

At first, we investigated the applicability of the core–shell material as a biocompatible drug delivery system by studying its biological properties. In order to verify the possibility of a practical use of the proposed material for biomedical applications, some in-depth in vitro cell tests were performed. For this purpose, the cytotoxicity and cell response of L929 fibroblast cells

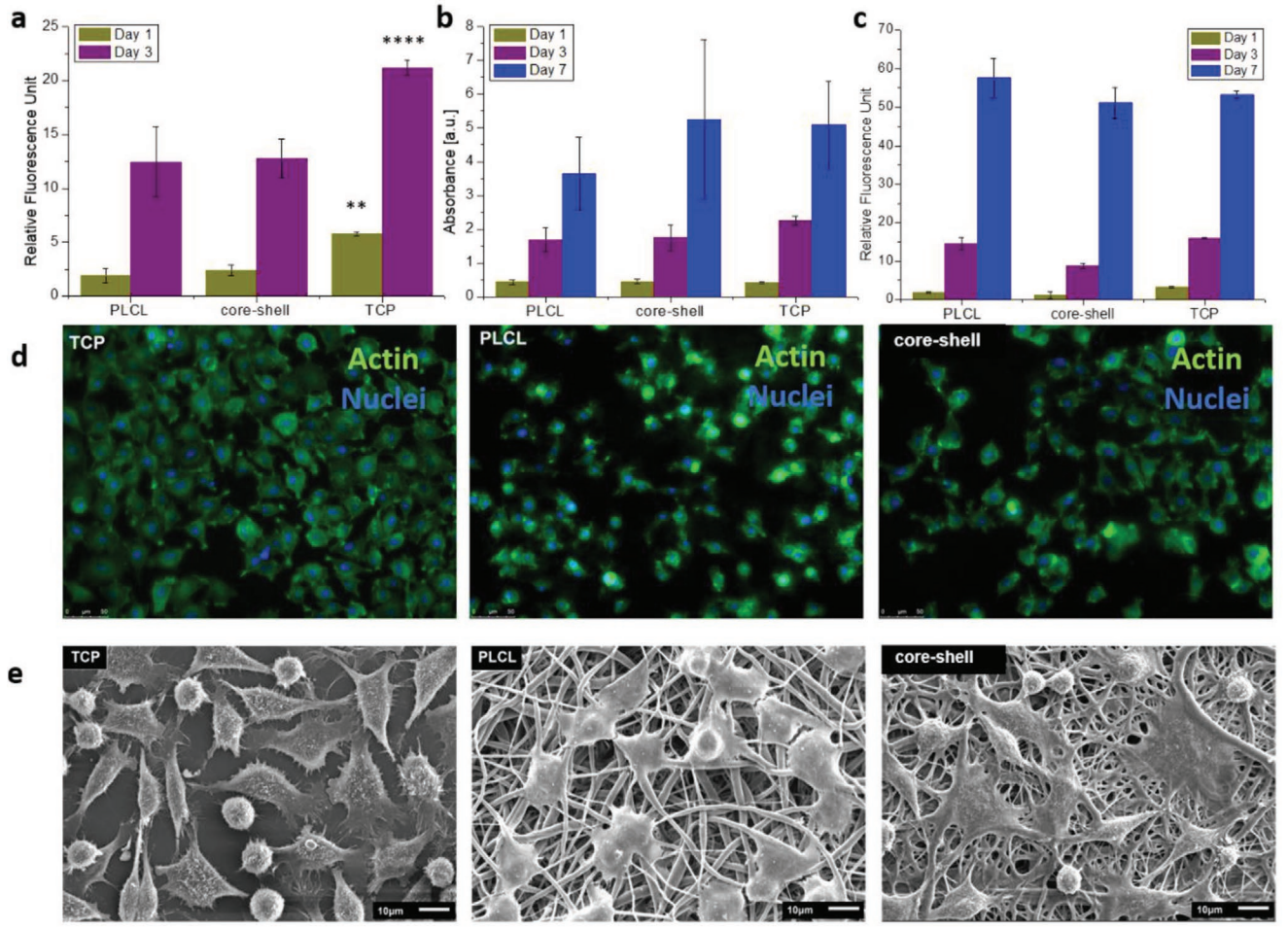

Figure 4. Biological responses of L929 fibroblasts cultured on PLCL fibers, P(NIPAAm-*co*-NIPMAAm)-PLCL core–shell fibers and TCP control. a) CyQuant DNA quantification of L929 cultured on the substrate having an increasing trend over the time for all tested conditions. b) Cell metabolic activity measured using the MTT test: values increased during the culture time in all the conditions tested. c) Cell proliferation measured with PrestoBlue assay: values increased over the culture time with no significant difference among the samples. Cell morphology: d) cell cytoskeleton and nuclei (actin/Hoachst 33342 staining) and e) cell SEM images. Cells spreads and elongates on the surface of both tested materials, showing the typical morphology of L929 fibroblasts.

cultured in direct contact with the materials were investigated, in terms of cell viability, metabolic activity and morphology. Cell viability was investigated using CyQuant assay measuring the DNA quantity on each sample. Data were collected from two time points, after 1 day to investigate on cell attachment, and after 3 days to evaluate the cell growth. **Figure 4**a shows that cells cultured on PLCL and P(NIPAAm-*co*-NIPMAAm)-PLCL fibrous materials attached and proliferated over the time, indicating that the scaffolds do not have negative effects on cell viability and function. Results were comparable for both types of fibrous materials during the culture time. However, fibroblasts cultured on the tissue culture plate (TCP) performed better at each time point. This is most probably due to the flat and smooth bulk TCP substrate which might allow a more efficient cell attachment and migration compared to more irregular and rough fibrous surfaces.[72,73] Subsequently, since cells are able to form and grow in a monolayer structure on TCP, they will easily have access to nutrients, resulting in higher rate of proliferation (Figure 4a). The metabolic activity and proliferation of fibroblasts cultured up to 7 days on core–shell material, PLCL fibrous scaffold and TCP were detected using 3-(4,5-dimethylthiazol-2-yl)-2,5-diphenyltetrazolium bromide (MTT) and PrestoBlue assays (Figure 4b,c, respectively). Data collected from the two tests were comparable for all the time points selected during the culture, reporting no significant difference among the tested conditions at any time point. Results show that cell metabolic activity and proliferation increased over the culture time, proving that both the fibrous materials provide a biomimetic micro-environment suitable for cell attachment and proliferation, without any toxic effect. We prove that cells proliferated, grew over time, and populated the scaffold, demonstrating the biocompatibility of these systems.

Changes in cell morphology during the culture time were analyzed using both SEM and fluorescent microscope. In addition, some more detailed information such as cellular adhesion and spreading on the materials were possible to be observed using field emission SEM (FE-SEM). Figure 4d illustrates actin/nuclei stained cells after 7 days of culture on PLCL and

P(NIPAAm-*co*-NIPMAAm)-PLCL core–shell fibers, showing elongated cytoskeletons of fibroblasts, proving the positive influence of the biomimetic structure of the analyzed materials on cell spreading. Results are supported by SEM images (Figure 4e), which proved that L929 cells achieved their typical morphology after 7 days of culture on both fibrous materials. However, it possible to observe that L929 fibroblasts seeded on P(NIPAAm-*co*-NIPMAAm)-PLCL core–shell fibers showed higher spreading compared to cells cultured on PLCL fibers. This difference in morphology, is probably related to the different architecture of the two samples. Indeed, PLCL and P(NIPAAm-*co*-NIPMAAm)-PLCL core–shell fibrous mats may show slightly different local porosity. Thus, different material porosity of the fibers influenced the morphology of seeded cells, as it has been also previously.[74] Moreover, SEM images in Figure S2, Supporting Information, show well developed filopodia of fibroblast cells attached to core–shell fibrous material. Taking into account all the imaging results, it is apparent that fibroblasts cultured on TCP and both fibrous materials achieved the clearly flattened and elongated cell morphology typical of fibroblasts. We can state that the core–shell material provides favorable conditions for the attachment, spreading and growth of fibroblasts, confirming the biocompatibility of the P(NIPAAm-*co*-NIPMAAm)-PLCL material. Our study proves that P(NIPAAm-*co*-NIPMAAm)-PLCL fibrous materials are good candidate substrates for growing cells, suggesting that this kind of material can be used for cell culture and tissue engineering applications, as well as for implantable drug delivery systems.

2.4. Self-Regulated Drug Delivery Mechanism of "Smart" Nanoplatforms

The ultimate objective of the present study was to develop thermo-responsive drug delivery systems based on cross-linked electrospun P(NIPAAm-*co*-NIPMAAm) nanofibers, stating that the release of bioactive molecules from cross-linked electrospun PNIPAAm nanofibers might be responsive to temperature changes. RhB is a fluorescent dye with a molecule size of 0.9 nm which is very often used as a drug model. Additionally, RhB is less expensive and easier to quantify with spectroscopic instruments than drugs with a similar diffusion coefficient.[75] Moreover, the majority of drug delivery models for electrospun fibers have been developed using RhB;[76,77] therefore, it is considered the best candidate, having a large spectrum of potential drug applications and offering the possibility to quantitatively compare our data with previous results.

Figure 5a shows the release of RhB from both PLCL fibrous structure and core–shell (P(NIPAAm-*co*-NIPMAAm)-PLCL) fibers, at three different temperatures. Significant differences in the release level were observed for the two types of materials tested. In the case of PLCL fiber material, after just 1 h of release at 24 °C, approximately 25% of the total mass of the dye trapped in the fiber structure was released. At 43 °C the release was over 60%. At a temperature of around 37 °C, we were dealing with the immediate release of RhB, and a plateau was reached after 24 h of release. At room temperature (24 °C) a significantly slower release was observed, which would asymptotically increase to 80%, as in the case for 37 and 43 °C. The reported graphs clearly show a higher degree of RhB release from fibrous polymer materials when the temperature is higher than 37 °C and a lower level of release when the temperature is lower than 37 °C. This is obviously associated with an increase in terms of desorption rate and further diffusional transport of RhB in nanopores when there is an increase in temperature. From the point of view of drug therapies, this phenomenon can result in a toxic effect at the initial stage due to the high concentration of bioactive molecules, followed by an inefficient drug release at the late stage (Figure 5b).[76]

In the case of core–shell fibers, release curves have a smoother trend and gradually reach values of around 20%, 25%, and 30% at 24, 37, and 43 °C, respectively, in up to 41 days of incubation (Figure 5a). Thus, when enclosing the hydrogel structure in a PLCL shell—which works as a porous membrane limiting the transport from the core—the release rate was significantly lower than in case of PLCL fibers. Moreover, we also did not observe such a large release of dye in the first hours as it was in case of PLCL fibers. This is a great step forward in the development of drug delivery nanosystems capable of avoiding any unwanted drug uptake just after the material implantation, and allowing an optimal drug supply during at both early and late stages (Figure 5b). By way of comparison, in the case of hydrogel material, the amount of the drug released decreases when temperature increases (Figure S3a, Supporting Information). A similar behavior was observed by Tsunomori and Ushiki.[78] They investigated the effect of pore size of P(NIPAAm-*co*-NIPMAAm) gel structure on the diffusion coefficient of RhB, proving their direct correlation. As indicated in the previous section, 37 °C is the typical P(NIPAAm-*co*-NIPMAAm) LCST. Above the LCST, the hydrogel shrinks and becomes dehydrated. This is a consequence of hydrogel conformation changes, which can result in a hydrogel volume phase transition from the hydrophilic, swollen state (T < LCST), to the hydrophobic, shrunken state (T > LCST).[79] The high environmental temperature in which the hydrogel was suspended causes its stronger and faster volume reduction. The pore size of the hydrogel structure also decreases, thus making it difficult to release the trapped RhB molecules from its structure. In addition, the diffusion coefficient of molecules within the hydrogel is much slower than in water at low temperatures.[80]

Surprisingly, in our study, when the hydrogel was confined within a polymer shell, a decreased release was not observed at temperatures higher than 37 °C. In the case of core–shell fibers, the presence of a PLCL shell plays a significant role in the mechanism of this unconventional drug delivery process. The glass transition temperature (T_g) of PLCL family can be individuated in a wide range of temperature, depending on monomer ratio, as well as synthesis temperature.[81] The T_g of pure poly(L-lactic acid) is around 60 °C, while pure polycaprolactone has a much lower T_g. By increasing the amount of caprolactone in the final copolymer, the T_g of PLCL copolymers can be easily reduced and adjusted according to the target.[82] In this case, the T_g of the copolymer is lower than the incubation temperature set during release tests. It is well-known that temperatures higher than T_g provoke changing in the mobility of the polymer matrix, inducing a more efficient transport of molecules though the matrix. Similar observations were made

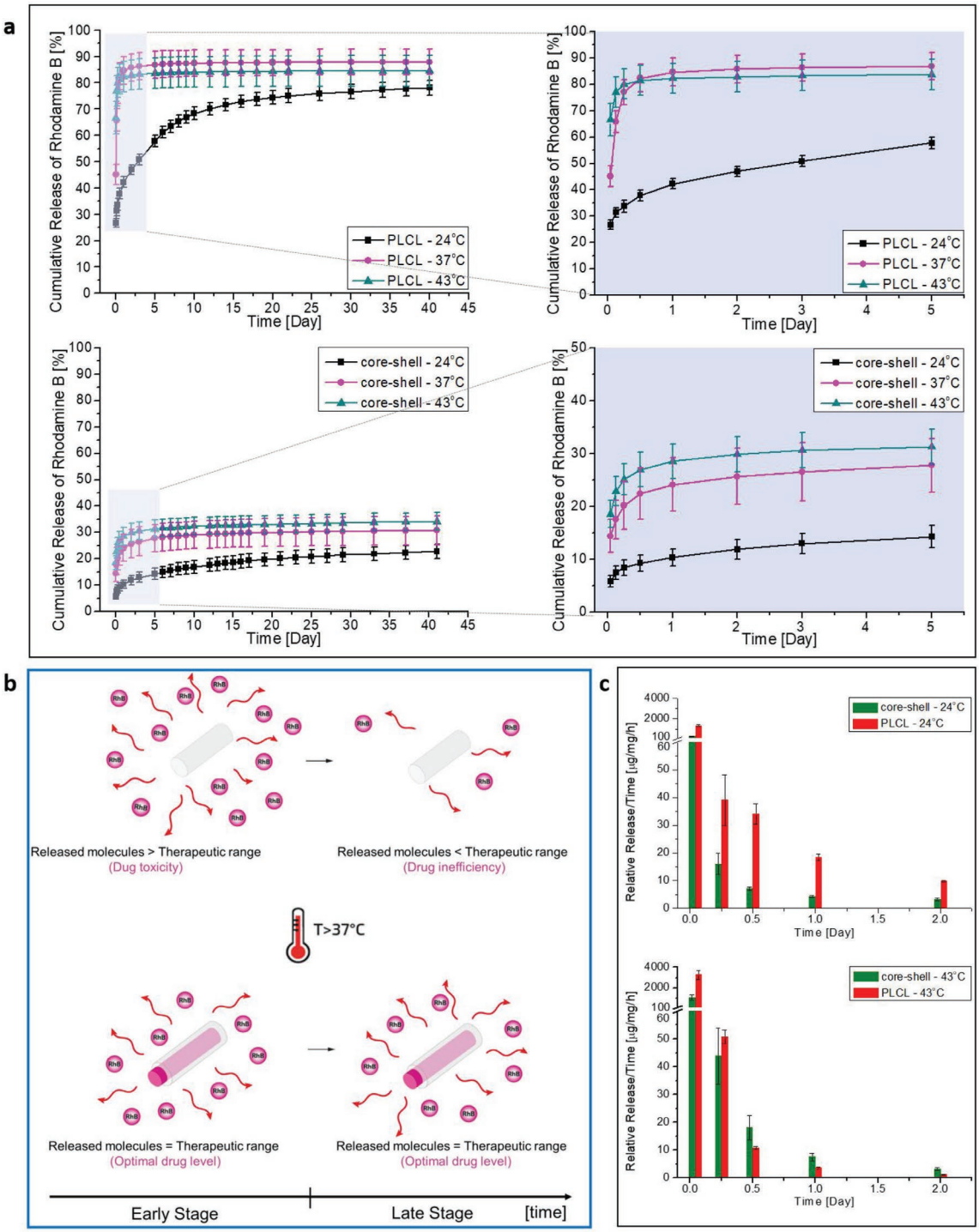

Figure 5. RhB release kinetics from PLCL fibers and P(NIPAAm-*co*-NIPMAAm)-PLCL core–shell fibers. a) Cumulative release of PLCL fibers and P(NIPAAm-*co*-NIPMAAm)-PLCL core–shell fibers incubated at 24, 37, and 43 °C for up to 41 days. After an initial burst release of around 80%, PLCL fibers reach a plateau after 24 h when incubated at 37 and 43 °C. In the case of a temperature of 24 °C, a slower release is reported, reaching a plateau of 70% after 400 h. The P(NIPAAm-*co*-NIPMAAm)-PLCL core–shell fiber system shows a more gradual release of around 20%, 25%, and 30% at 24, 37, and 43 °C, respectively, in up to 41 days of incubation. b) Schematic of thermo-responsive release at 37 °C: at the early incubation stage the PLCL fiber system releases a large quantity of RhB, at later stages it releases very few molecules. The P(NIPAAm-*co*-NIPMAAm)-PLCL core–shell fiber system releases a suitable quantity of RhB molecules within the therapeutic range at both early and late stages. c) Relative release of PLCL fibers and P(NIPAAm-*co*-NIPMAAm)-PLCL core–shell fibers at early incubation stages (up to 50 h) at 24 and 43 °C. A significantly higher level of dye was released from PLCL fibers than from core–shell fibers in case of room temperature. At a higher temperature and during the incubation time this trend gradually reversed detecting a higher release from the core–shell than from PLCL fibers.

by Yu and co-authors during investigation of PNIPAAm-ethyl cellulose core–shell microspheres.[80] It is suggested that the presence of the hydrogel core increases the diffusion resistance of dye molecules, which slows down the release of RhB from the system. A further analysis shows that at room temperature (24 °C), a significantly higher level of dye was released from PLCL fibers than from core–shell fibers (Figure 5c). These values were at least twice as high in favor of PLCL. As the temperature and release time increased, these differences gradually decreased until the dependence was reversed—more RhB was released from core–shell fibers than from PLCL fibers. For instance, after only 12 h at 43 °C, PLCL fibers released 80% of the dye while the core–shell released approximately 27% (Figure 5c). At a temperature of 37 °C and after a 24-h incubation, the level of release of both materials was similar, and subsequently higher for the core–shell fibrous mat at each next time point (Figure S3b, Supporting Information). An additional advantage of core–shell fiber mats as a controlled drug release system is the extended release time. After 41 days of release, RhB was no longer present in the supernatant for PLCL nanofibers. After the same release time (at each investigated temperature), a small continuous release of dye from core–shell mats was detected (Figure S3c, Supporting Information).

An important parameter which may affect the drug release rate from core–shell fibers is PLCL shell thickness. Various strategies to control the thickness of core–shell architecture can be found in the literature, including modulation of flow rate of shell[83] and core[84,85] polymers. The strategy we adopted, combining those two, relies on establishing the correct ratio between shell and core flow rate.[86] It is well-known that increasing of the shell flow, the thickness of the shell increases,[83] while when the core flow increases, a decreasing of shell thickness is observed.[84,85] In this case, we optimized simultaneously the flow rate of core and shell components, obtaining core–shell fibers with the desired structure (e.g., continuous core), size and drug release properties. We state that the polymer shell coating on the hydrogel core could reduce the release of molecules at the early stage. The PLCL shell acted as an additional barrier, thus limiting the amount of the dye released from the core–shell fiber structure compared to simple fibrous hydrogel systems.[52] RhB molecules were gradually diffusing through the shell structure and escaped through its surface. The diffusion rate strongly depends on the temperature—the higher the temperature, the higher the diffusion coefficient of RhB molecules and, consequently, the higher the concentration of released RhB over time.

In summary, two factors control the release rate of the substance entrapped in the core–shell structure. The first is the temperature, which affects the hydrogel core. During dehydration, the water expelled drags dye molecules out from the core, while the diffusional transport through the shell layer increases. The second factor is the hierarchical structuration of nanofibers, especially the shell properties (e.g., thickness and composition).[87]

The core–shell nanofiber system developed is able to self-regulate drug delivery, thus avoiding an excessive and dangerous release of bioactive molecules during the first stage of drug administration, while extending the delivery time. This strategy opens up great opportunities in the development of brand-new drug delivery systems, in which the time and rate of release are controlled on several levels: by designing the composition of the hydrogel (the quantitative content of individual monomers and cross-linker strongly affect the porosity and drug diffusion), and its hierarchical structure (determining the approximate shell structure and composition).

3. Conclusion

In summary, for the first time, we have reported on the successful fabrication of an electrospun hierarchical-structured nanoplatform based on fully cross-linked P(NIPAAm-*co*-NIPMAAm) hydrogel with biomimetic structural properties for the self-regulated delivery of drugs. The core–shell fibrous mat was fabricated by a custom-designed co-axial electrospinning technique assisted by an in situ UV light-triggered free-radical cross-linking polymerization under controlled environmental conditions and followed by a post-electrospinning treatment. We have shown that the release rate of our system was self-programmable, thanks to the presence of both a thermoresponsive hydrogel core loaded with a drug model and a PLCL shell that acted as both a protective layer and a reservoir during the release. The role of the hydrogel core is vital in the regulation mechanism, since it undergoes reversible physical changes upon exceeding the normal body temperature (e.g., during diseases or inflammation). P(NIPAAm-*co*-NIPMAAm) hydrogel system has a typical LCST of around 37 °C, like the human body temperature, making it possible for the system to thermally induce the drug delivery self-regulation. In addition, the hydrogel is encapsulated within a PLCL shell in order to limit the release of the drug model. The polymeric shell is designed not only to make possible the formation of nanofibers during electrospinning, but also to mimic the native ECM, thus improving the cell–material interaction. To study the controlled functions of the "smart" drug delivery system to release drugs, RhB was chosen, since it is one of the most used drug models. Nanofiber responsiveness was investigated by means of a series of analyses performed at different temperatures. The core–shell hydrogel-based nanofibrous material showed a temperature-dependent drug delivery kinetics, in which the drug model release is driven by a temperature-controlled desorption. The system developed paves the way for the development of fully cross-linked electrospun polyacrylate hydrogel-based nanofibers which make it possible to expand the electrospinning capabilities beyond traditional structures. The final electrospun nanoplatform has great potential within the framework of self-regulated drug delivery, and appears promising for various clinical applications, especially to overcome issues connected with the inability to achieve therapeutic levels and/or to avoid nonspecific drug uptake in healthy tissues during bioactive molecule delivery.

4. Experimental Section

Materials: Core–shell nanofibers were produced and subsequently analyzed using the following materials without any further modification: poly-L-lactide-*co*-caprolactone (PLCL, 70% L-lactide and 30% caprolactone, Corbion Purac, Netherlands), chloroform ($CHCl_3$, POCh, Poland), *N*,*N*-dimethylformamide (DMF, POCh, Poland),

N-isopropylacrylamide (NIPAAm, 97%, Sigma-Aldrich, Poland), *N*,*N*′-methylene bisacrylamide (BIS-AAm, 99.5%, Sigma-Aldrich, Poland), *N*-isopropylmethacrylamide (NIPMAAm, 97%, Sigma-Aldrich, Poland), 2-hydroxy-4′-(2-hydroxyethoxy)-2-methylpropiophenone (Irgacure 2959, 98%, Sigma-Aldrich, Poland), ammonium persulfate (APS, 98%, Sigma-Aldrich, Poland), *N*,*N*,*N*′,*N*′-tetramethylethylenediamine (TEMED, 99%, Sigma-Aldrich, Poland), RhB (95%, Sigma-Aldrich, Poland), mouse fibroblasts (L929, Sigma-Aldrich ATTC), DMEM (phenol red, L-glutamine, high glucose, no sodium pyruvate, ThermoFisher Scientific), fetal bovine serum (FBS, F9665, Sigma-Aldrich), 1% antibiotic (penicillin/streptomycin), PrestoBlue cell viability reagent (Invintrogen, ThermoFisher Scientific), 3-(4,5-dimethylthiazol-2-yl)-2,5-diphenyltetrazolium bromide assay (MTT, ThermoFisher Scientific), CyQuant assey (ThermoFisher Scientific), glutaraldehyde (25%, Sigma-Aldrich, Poland), hexadimetylosiloxane (HDMS, 98,5%, Sigma-Aldrich, Poland), ethanol (POCh, Poland), paraformaldehyde (PFA, 95%, Sigma-Aldrich, Poland), Triton X-100 (Sigma-Aldrich, Poland), Actin Green (Invintrogen, ThermoFisher Scientific), NucBlue Live ReadyProbes Reagent (Invintrogen, ThermoFisher Scientific), ActinGreen 488 ReadyProbes Reagent (Invintrogen, ThermoFisher Scientific), PBS (Sigma-Aldrich, Poland), isopropanol (POCh, Poland), and hydrochloric acid (HCl, POCh, Poland).

Sample Preparation: The shell polymer solution was prepared by dissolving 1 g of PLCL in 10 g of a mixture of $CHCl_3$ and DMF 9:1 (w/w). The hydrogel core solution (10 wt%) was a mixture of 0.876 g of NIPAAm, 0.025 g of NIPMAAm, 0.1 g of BIS-AAm, 0.01 g of photoinitiator (Irgacure 2959), and 10 mL of deionized water. A photoinitiator was used to trigger the hydrogel polymerization reaction upon UV irradiation, while BIS-AAm was the hydrogel system cross-linker. Before spinning, the hydrogel precursor solution was bubbled with argon gas for 10 min. To increase the viscosity of the hydrogel precursor solution in electrospinning, a small amount of APS and TEMED was added to a final concentration of 2 and 0.4 µL mL^{-1}, respectively. Custom-made co-axial electrospinning equipment was used for the fabrication of core–shell nanofibers. Furthermore, an additional source of UV radiation was installed in the electrospinning chamber in the form of an optical fiber connected to a mercury lamp to shine UV light directly onto the collector where the fibers were collected during the process. The chamber was additionally equipped with a temperature control system, which ensured that the spinning took place in strictly defined conditions, providing fibers with specific parameters. Core–shell fibers were electrospun using 15 kV positive voltage and a flow rate of 300 µL h^{-1} for the core solution and 800 µL h^{-1} for the shell solution. A custom-made co-axial needle was used, with a 21G needle for the core and a 15G needle for the shell. Fibers were collected on a grounded drum rotating at 500 rpm and placed 20 cm away from the needle. The typical temperature and humidity in electrospinning were below 20 °C and above 70%, respectively. High humidity is crucial for spinning core–shell fibers with aqueous core solution, while temperature control is important to prevent exceeding the LCST (37 °C for P(NIPAAm-*co*-NIPMAAm)), so there is no loss of water by the hydrogel core or inhomogeneity during the polymer cage formation. After electrospinning, the core–shell mat was additionally irradiated under a UV lamp (density of power 225 mW cm^{-2}) for 2 min with cooling of the irradiated sample. Core–shell fibrous materials containing a drug model were fabricated using the same procedure and adding 5 mg of RhB in 5 mL of the hydrogel precursor solution during the early stage of preparation. In addition, PLCL nanofibers with RhB were prepared as a reference material. The polymer solution was prepared in exactly the same way as the shell polymer solution, with a quantity of RhB reaching at 1 wt%. of the total polymer mass. A single needle (26G) was used as spinneret. Electrospinning parameters were set at 15 kV positive voltage, 800 µL h^{-1} flow rate, needle-collector distance of 20 cm, 500 rpm of drum rotation, temperature of 24 °C, and humidity of 70%.

Morphological Analysis: In order to visualize the presence of the core, fluorescein-o-acrylate was added in the hydrogel precursor (0.1 mg mL^{-1}). The core–shell structure of the fibers was observed by using an inverted epifluorescence microscope (Leica AM TIRF MC) with a set of microscopic lens (20×/0.40 CORR, 63×/0.70 CORR), an appropriate set of filters (Leica GFP ET, excitation 450–490 nm, emission 500–550 nm), and a mercury lamp (Leica EL6000) as a source for fluorescence excitation.

SEM was used to analyze the size and shape of core–shell and pure PLCL fibers. SEM and FE-SEM images were observed using JEOL JSM-6390LV and FEI Nova NanoSEM 450 microscopes with an accelerating voltage of 10 kV. Before imaging, nanofibrous mats were coated with a 8 nm-thick gold layer. The distribution of the fiber diameter was determined using at least 100 measurements for each sample. This technique was also useful for the observation of the partially dissolved shell layer. TEM was used to prove the presence of a core–shell structure. TEM analysis was conducted on the Jeol JEM-1011 at an accelerated voltage of 80 kV. The core–shell fibers were electrospun on a TEM Cu grid with 300 mesh. In order to analyze the sample morphology, AFM was used for additional measurements. Five fibers from five different sample areas were measured using an AFM (Ntegra, NT-MDT) equipped with a silicon cantilever with a 6 nm nominal tip radius (NSG01, NT-MDT) in a semicontact mode, with a resonance frequency of 150 kHz and 500 × 500 points per image. Before this analysis, the core–shell samples (fibers deposited on a glass slide) were immersed in deionized water for one day to fully hydrate the hydrogel core, and the experiment was performed at room temperature.

Characterization Methods: DSC was performed using a Perkin Elmer PYRIS-1 unit and data were analyzed using Origin 8 software. DSC made it possible to determinate hydrogel LCST and the degree of crystallinity of the materials fabricated. Measurements were performed in heating and cooling modes from −30 to 200 °C, at a rate of 10 °C min^{-1} with 5-min isothermal stops at the beginning and end of the heating mode. The sample weight was approximately 5 mg. The T_g was determined at the deflection point, while the melting temperature (T_m) was determined at a peak maximum point, both in cooling mode. WAXS was performed with a Bruker D8 Discover diffractometer in the reflection mode, using Bragg-Brentano geometry. The analysis was conducted in the angular range (2 theta, 2θ) between 5° and 31°. Data were collected with a step of 0.02° per 1.0 s at each point. FTIR spectroscopy was used for the characterization of the present material functional groups. FTIR analysis was conducted in the attenuated total reflectance (ATR) mode with a Bruker Vertex70 FT-IR Spectrometer, and carried out in the wavenumbers range of 400–4000 cm^{-1} with a resolution of 2 cm^{-1} and 12 scans for each sample. In the case of P(NIPAAm-*co*-NIPMAAm), the samples were characterized by ATR-FTIR using the freeze-dried hydrogel.

In Vitro Biocompatibility Tests: In order to study the cellular response to nanofibrous materials, a series of different biological tests were performed using mouse fibroblasts (L929, Sigma-Aldrich ATTC) cultured on P(NIPAAm-*co*-NIPMAAm)-PLCL and PLCL scaffolds as well as TCP. All materials were cut into squares (1 cm^2 each, suitable for 48 well plates), sterilized by UV light (30 min on each side), and seeded with cells with density of 8000 units cm^{-2}. Samples were cultured in a medium consisting of DMEM (phenol red, L-glutamine, high glucose, no sodium pyruvate, ThermoFisher Scientific) modified with 10% FBS (F9665, Sigma-Aldrich), and 1% antibiotic (penicillin/streptomycin). A CyQuant assay was performed at days 1 and 3 of culture to measure the DNA content on each surface in order to investigate the cell viability and subsequent growth. In each time point, before the CyQuant assay, the samples were rinsed with PBS and stored in −75 °C, until the measurement was performed. Directly before the analysis, the dye solution was prepared using water, cell-lysis buffer (5%) and CyQuant GR (0,25%) dye, according to the protocol. 200 µL of this solution was added to the samples, previously warmed up to the ambient temperature. After 5 min, the data were collected using fluorescence, with excitation in 480 nm and emission at 520 nm. On the other hand, to evaluate the viability and the mitochondrial metabolic activity MTT and PrestoBlue assays were performed. In order to investigate the cell proliferation, the tests were repeated after 1, 3, and 7 days of cell culture. In vitro experiments were conducted on 5 samples of each material. For quantitative measurements, three repetition for each sample were done. In order to perform MTT assay, after each time point, the culture

medium was removed and directly replaced with solution containing: medium (300 µL) and terazolium dye (100 µL). Later, the samples were incubated per 3 h at 37 °C. Finally, the medium with dye was removed and replaced with izopropanol. After 10 min washing, the formazan from the samples, 130 µL of each sample was transferred to 96-well plate in order to measure the absorbance. Absorbance was measured at a 570 nm wavelength using a MultiskanGO Microplate Spectrophotometer (Thermo Fisher Scientific, USA). For PrestoBlue test, after removing the culture medium, 10% solution of resazulin dye solution was added to the samples, 360 µL culture medium and 40 µL of resazulin dye solution. Cell incubation time in PrestoBlue solution (Invintrogen) was set to 1 h. The data were collected using fluorescence, with excitation in 530 nm and emission at 620 nm. The characterization of cellular morphology was studied by SEM imaging and optical fluorescent microscopy. For SEM imaging, samples were incubated in 2.5% GTA for 0.5 h and dehydrated sequentially with three different concentration of ethanol solutions (60%, 80%, 100%) for 15 min each. Then, samples were incubated for 15 min in differently proportioned ethanol/hexadimetylosiloxane solutions (1:2, 1:1, 2:1), and finally with 100% hexadimetylosiloxane. At the end, samples were let dry under the fume hood. Samples were then coated with sputtered gold and imaged using both SEM and FE-SEM microscopes. The samples addressed to fluorescent microscopy were fixed with 3% PFA solution for 30 min. Afterward, cell membrane permeability was increased by immersing samples in Triton X-100 for 5 min. Finally, samples were immersed in ActinGreen and NucBlue Reagent (Invintrogen), incubated for 30 min, rinsed in PBS, and imaged on a Leica DMI3000B fluorescent microscope.

Drug Release Experiment: The RhB release from two types of materials—core–shell fibrous mats and PLCL mats—was analyzed. RhB concentration in nanofibrous mats was set to 1 wt% of the total polymer weight. In the case of core–shell materials, RhB was added to the hydrogel precursor solution, while for PLCL mats, RhB was added to the polymer solution before electrospinning. The release process was performed at three different temperatures: room temperature (24 °C), 37 °C, and 43 °C. Core–shell nanofibrous and PLCL mats (1 cm^2 of each) were weighed to determine RhB contents and immersed in 1 mL of deionized water at the same temperatures mentioned above. The supernatant fluid was removed after 1, 3, 6, 12, and 24 h of release and exchanged with fresh water. Over the next few weeks, the release level of RhB was measured after every 24 h. Subsequently, the measurement time points were ultimately increased to once per week. A fluorometer (Fluoroskan Ascent Microplate Fluorometer, Thermo Scientific, USA) was used to evaluate the concentration of the released RhB from the fibrous mats (e.g., core–shell, PLCL) based on the calibration curve. The data were collected with excitation in 485 nm, emission at 538 nm. All release experiments were repeated at least six times for each temperature.

Statistical Analysis: Data were displayed as means ± standard deviation. If not specified, experiments were performed in quintuplicates. Statistical significance of the data was determined using one way single factorial analysis of variance (ANOVA). The *p*-values were considered as significant differences when $p < 0.05$ (**$p < 0.01$, ****$p < 0.0001$).

Supporting Information

Supporting Information is available from the Wiley Online Library or from the author.

Acknowledgements

S.P. and C.R. contributed equally to this work. This work was supported by the National Science Centre grant no. 2015/19/D/ST8/03196. F.P. and P.N. acknowledge the financial support of the Polish Ministry of Science and Higher Education obtained through scholarships for outstanding young scientists. Part of this research was also carried out with the use of apparatuses available thanks to the EC structural funds within the framework of the Center for Preclinical Research and Technology (CePT), POIG Nr. 02.02.00-17-024/08-00.

Conflict of Interest

The authors declare no conflict of interest.

Keywords

biomimetic nanomaterials, electrospun core–shell nanofibers, hierarchical nanostructures, smart drug delivery, thermo-responsive hydrogels

Received: February 12, 2020
Revised: March 26, 2020
Published online:

[1] L. L. Hench, *Biomaterials* **1998**, *19*, 1419.
[2] E. C. Gil, A. I. Colarte, B. Bataille, J. L. Pedraz, F. Rodríguez, J. Heinämäki, *Int. J. Pharm.* **2006**, *317*, 32.
[3] M. Hadjianfar, D. Semnani, J. Varshosaz, *Polym. Adv. Technol.* **2018**, *29*, 2972.
[4] M. Chen, Y.-F. Li, F. Besenbacher, *Adv. Healthcare Mater.* **2014**, *3*, 1721.
[5] Q. Wei, A. Wei, in *Functional Nanofibers and Their Applications*, Vol. *8* (Ed: Q. Wei), Woodhead Publishing, Philadelphia, PA **2012**, Ch. 8.
[6] G. Piccirillo, D. A. Carvajal Berrio, A. Laurita, A. Pepe, B. Bochicchio, K. Schenke-Layland, S. Hinderer, *Sci. Rep.* **2019**, *9*, 3446.
[7] S. Thakkar, M. Misra, *Eur. J. Pharm. Sci.* **2017**, *107*, 148.
[8] Y.-C. Li, Y. S. Zhang, A. Akpek, S. R. Shin, A. Khademhosseini, *Biofabrication* **2016**, *9*, 012001.
[9] F. Pierini, P. Nakielski, O. Urbanek, S. Pawłowska, M. Lanzi, L. De Sio, T. A. Kowalewski, *Biomacromolecules* **2018**, *19*, 4147.
[10] A. Merlettini, M. Gigli, M. Ramella, C. Gualandi, M. Soccio, F. Boccafoschi, M. L. Focarete, *Biomacromolecules* **2017**, *18*, 2499.
[11] J. G. Hardy, M. Palma, S. J. Wind, M. J. Biggs, *Adv. Mater.* **2016**, *28*, 5717.
[12] S. Zeng, R. Li, S. G. Freire, V. M. M. Garbellotto, E. Y. Huang, A. T. Smith, C. Hu, W. R. T. Tait, Z. Bian, G. Zheng, D. Zhang, L. Sun, *Adv. Mater.* **2017**, *29*, 1700828.
[13] F. Guo, Z. Guo, *RSC Adv.* **2016**, *6*, 36623.
[14] M. Raisch, D. Genovese, N. Zaccheroni, S. B. Schmidt, M. L. Focarete, M. Sommer, C. Gualandi, *Adv. Mater.* **2018**, *30*, 1802813.
[15] M. Kanamala, W. R. Wilson, M. Yang, B. D. Palmer, Z. Wu, *Biomaterials* **2016**, *85*, 152.
[16] Y. Wang, G. Wei, X. Zhang, F. Xu, X. Xiong, S. Zhou, *Adv. Mater.* **2017**, *29*, 1605357.
[17] E. M. Ahmed, *J. Adv. Res.* **2015**, *6*, 105.
[18] H. L. Lim, Y. Hwang, M. Kar, S. Varghese, *Biomater. Sci.* **2014**, *2*, 603.
[19] E. Prince, E. Kumacheva, *Nat. Rev. Mater.* **2019**, *4*, 99.
[20] E. Caló, V. V. Khutoryanskiy, *Eur. Polym. J.* **2015**, *65*, 252.
[21] A. Vashist, A. Vashist, Y. K. Gupta, S. Ahmad, *J. Mater. Chem. B* **2014**, *2*, 147.
[22] H. A. Al-Mohsin, K. P. Mineart, R. J. Spontak, *Adv. Energy Mater.* **2015**, *5*, 1401941.
[23] Z. Qiao, H. Zhang, S. Karakalos, S. Hwang, J. Xue, M. Chen, D. Su, G. Wu, *Appl. Catal., B* **2017**, *219*, 629.
[24] X. Bai, Y. Yu, H. H. Kung, B. Wang, J. Jiang, *J. Power Sources* **2016**, *306*, 42.

[25] Q. Xu, Z. Zhang, C. Xiao, C. He, X. Chen, *Biomacromolecules* **2017**, *18*, 1411.
[26] J. G. Torres-Rendon, T. Femmer, L. De Laporte, T. Tigges, K. Rahimi, F. Gremse, S. Zafarnia, W. Lederle, S. Ifuku, M. Wessling, J. G. Hardy, A. Walther, *Adv. Mater.* **2015**, *27*, 2989.
[27] Y. Guan, Y. Zhang, *Soft Matter* **2011**, *7*, 6375.
[28] C. D. Spicer, *Polym. Chem.* **2020**, *11*, 184.
[29] S. Pawłowska, P. Nakielski, F. Pierini, I. K. Piechocka, K. Zembrzycki, T. A. Kowalewski, *PLoS One* **2017**, *12*, e0187815.
[30] S. Ashraf, H.-K. Park, H. Park, S.-H. Lee, *Macromol. Res.* **2016**, *24*, 297.
[31] Z. Liu, Y. Faraj, X.-J. Ju, W. Wang, R. Xie, L.-Y. Chu, *J. Polym. Sci., Part B: Polym. Phys.* **2018**, *56*, 1306.
[32] N. M. Oliveira, C. Martins-Cruz, M. B. Oliveira, R. L. Reis, J. F. Mano, *Adv. Biosyst.* **2018**, *2*, 1700069.
[33] S. Pawłowska, T. A. Kowalewski, F. Pierini, *Soft Matter* **2018**, *14*, 8421.
[34] P. Nakielski, F. Pierini, *Acta Biomater.* **2019**, *84*, 63.
[35] L. Wang, Y. Qiu, H. Lv, Y. Si, L. Liu, Q. Zhang, J. Cao, J. Yu, X. Li, B. Ding, *Adv. Funct. Mater.* **2019**, *29*, 1901407.
[36] S. Hinderer, S. L. Layland, K. Schenke-Layland, *Adv. Drug Delivery Rev.* **2016**, *97*, 260.
[37] S. Metwally, J. E. Karbowniczek, P. K. Szewczyk, M. M. Marzec, A. Gruszczyński, A. Bernasik, U. Stachewicz, *Adv. Mater. Interfaces* **2019**, *6*, 1801211.
[38] O. Urbanek, P. Sajkiewicz, F. Pierini, *Polymer* **2017**, *124*, 168.
[39] P. K. Szewczyk, S. Metwally, J. E. Karbowniczek, M. M. Marzec, E. Stodolak-Zych, A. Gruszczyński, A. Bernasik, U. Stachewicz, *ACS Biomater. Sci. Eng.* **2019**, *5*, 582.
[40] D. H. Reneker, A. L. Yarin, *Polymer* **2008**, *49*, 2387.
[41] Y. Lai, Y. Zhao, W. Cai, J. Song, Y. Jia, B. Ding, J. Yan, *Small* **2019**, *15*, 1905171.
[42] D. H. Reneker, A. L. Yarin, E. Zussman, H. Xu, *Adv. Appl. Mech.* **2007**, *41*, 345.
[43] F. Pierini, M. Lanzi, P. Nakielski, S. Pawłowska, O. Urbanek, K. Zembrzycki, T. A. Kowalewski, *Macromolecules* **2017**, *50*, 4972.
[44] A. Camposeo, R. Jurga, M. Moffa, A. Portone, F. Cardarelli, F. D. Sala, C. Ciracì, D. Pisignano, *Small* **2018**, *14*, 1800187.
[45] Z. Sun, E. Zussman, A. L. Yarin, J. H. Wendorff, A. Greiner, *Adv. Mater.* **2003**, *15*, 1929.
[46] H. Zhang, Q. Niu, N. Wang, J. Nie, G. Ma, *Eur. Polym. J.* **2015**, *71*, 440.
[47] A. S. Ranganath, V. A. Ganesh, K. Sopiha, R. Sahay, A. Baji, *RSC Adv.* **2017**, *7*, 19982.
[48] C.-L. Zhang, F.-H. Cao, J.-L. Wang, Z.-L. Yu, J. Ge, Y. Lu, Z.-H. Wang, S.-H. Yu, *ACS Appl. Mater. Interfaces* **2017**, *9*, 24857.
[49] E. Schoolaert, P. Ryckx, J. Geltmeyer, S. Maji, P. H. M. Van Steenberge, D. R. D'hooge, R. Hoogenboom, K. De Clerck, *ACS Appl. Mater. Interfaces* **2017**, *9*, 24100.
[50] L. Wang, Y. Wu, B. Guo, P. X. MA, *ACS Nano* **2015**, *9*, 9167.
[51] L. Wang, Y. Wu, T. Hu, P. X. Ma, B. Guo, *Acta Biomater.* **2019**, *96*, 175.
[52] Z. Wei, W. Zhao, Y. Wang, X. Wang, S. Long, J. Yang, *Colloids Surf., B* **2019**, *182*, 110347.
[53] M. A. Haq, Y. Su, D. Wang, *Mater. Sci. Eng., C* **2017**, *70*, 842.
[54] Y. Ono, T. Shikata, *J. Am. Chem. Soc.* **2006**, *128*, 10030.
[55] T. Kanai, D. Lee, H. C. Shum, D. A. Weitz, *Small* **2010**, *6*, 807.
[56] M. K. Kokufuta, S. Sato, E. Kokufuta, *Colloid Polym. Sci.* **2012**, *290*, 1671.
[57] L. Starovoytova, J. Spěváček, M. Ilavský, *Polymer* **2005**, *46*, 677.
[58] F. Y. Pong, M. Lee, J. R. Bell, N. T. Flynn, *Langmuir* **2006**, *22*, 3851.
[59] T. Ikeda-Fukazawa, N. Ikeda, M. Tabata, M. Hattori, M. Aizawa, S. Yunoki, Y. Sekine, *J. Polym. Sci., Part B: Polym. Phys.* **2013**, *51*, 1017.
[60] K. Kratz, T. Hellweg, W. Eimer, *Polymer* **2001**, *42*, 6631.
[61] J. Xue, T. Wu, Y. Dai, Y. Xia, *Chem. Rev.* **2019**, *119*, 5298.
[62] W.-H. Lin, W.-B. Tsai, *Biofabrication* **2013**, *5*, 035008.
[63] P. Nakielski, S. Pawlowska, F. Pierini, V. Liwinska, P. Hejduk, K. Zembrzycki, E. Zabost, T. A. Kowalewski, *PLoS One* **2015**, *10*, e0129816.
[64] K. Garkhal, S. Verma, S. Jonnalagadda, N. Kumar, *J. Polym. Sci., Part A: Polym. Chem.* **2007**, *45*, 2755.
[65] C. A. Ribeiro, M. V. S. Martins, A. H. Bressiani, J. C. Bressiani, M. E. Leyva, A. A. A. de Queiroz, *Mater. Sci. Eng., C* **2017**, *81*, 156.
[66] C. S. Biswasa, K. Mitraa, S. Singha, D. K. Patelb, B. Maitia, P. Maitib, B. Ray, *J. Chem. Sci.* **2016**, *128*, 941.
[67] D. Zhu, M. Lu, J. Guo, L. Liang, Y. Lan, *J. Appl. Polym. Sci.* **2012**, *124*, 155.
[68] S. A. Jadhav, V. Brunella, I. Miletto, G. Berlier, D. Scalarone, *J. Appl. Polym. Sci.* **2016**, *133*, 44181.
[69] A. Evanghelidis, M. Beregoi, V. C. Diculescu, A. Galatanu, P. Ganea, I. Enculescu, *Sci. Rep.* **2018**, *8*, 17555.
[70] P. Roach, D. J. McGarvey, M. R. Lees, C. Hoskins, *Int. J. Mol. Sci.* **2013**, *14*, 8585.
[71] J. Song, B. Sun, S. Liu, W. Chen, Y. Zhang, C. Wang, X. Mo, J. Che, Y. Ouyang, W. Yuan, C. Fan, *Front. Mol. Neurosci.* **2016**, *9*, 117.
[72] S. Murikipudi, H. Methe, E. R. Edelman, *Biomaterials* **2013**, *34*, 677.
[73] N. Khosravi, A. Maeda, R. S. DaCosta, J. E. Davies, *Commun. Biol.* **2018**, *1*, 72.
[74] J. Rnjak-Kovacina, S. G. Wise, Z. Li, P. K. M. Maitz, C. J. Young, Y. Wang, A. S. Weiss, *Biomaterials* **2011**, *32*, 6729.
[75] P. Nakielski, T. Kowalczyk, K. Zembrzycki, T. A. Kowalewski, *J. Biomed. Mater. Res., Part B* **2015**, *103*, 282.
[76] R. Srikar, A. L. Yarin, C. M. Megaridis, A. V. Bazilevsky, E. Kelley, *Langmuir* **2008**, *24*, 965.
[77] M. Gandhi, R. Srikar, A. L. Yarin, C. M. Megaridis, R. A. Gemeinhart, *Mol. Pharmaceutics* **2009**, *6*, 641.
[78] F. Tsunomori, H. Ushiki, *Phys. Lett. A* **1999**, *258*, 171.
[79] L. Chu, R. Xie, X. Ju, *Chin. J. Chem. Eng.* **2011**, *19*, 891.
[80] Y.-L. Yu, M.-J. Zhang, R. Xie, X.-J. Ju, J.-Y. Wang, S.-W. Pi, L.-Y. Chu, *J. Colloid Interface Sci.* **2012**, *376*, 97.
[81] J. Fernández, A. Etxeberria, J. R. Sarasua, *J. Mech. Behav. Biomed. Mater.* **2012**, *9*, 100.
[82] J. Brostrom, A. Boss, I. S. Chronaki, *Biomacromolecules* **2004**, *5*,1124.
[83] K. T. Shalumon, G. J. Lai, C. H. Chen, J. P. Chen, *ACS Appl. Mater. Interfaces* **2015**, *7*, 21170.
[84] C. Wang, K. W. Yan, Y. D. Lin, P. C. H. Hsieh, *Macromolecules* **2010**, *43*, 6389.
[85] H. Jiang, Y. Hu, Y. Li, P. Zhao, K. Zhu, W. Chen, *J. Controlled Release* **2005**, *108*, 237.
[86] Y. Su, Q. Su, W. Liu, M. Lim, J. R. Venugopal, X. Mo, M. El-Newehy, *Acta Biomater.* **2012**, *8*, 763.
[87] S. F. Chou, D. Carson, K. A. Woodrow, *J. Controlled Release* **2015**, *220*, 584.